



ELSEVIER

Journal of Electron Spectroscopy and Related Phenomena 119 (2001) 161–174

JOURNAL OF  
ELECTRON SPECTROSCOPY  
and Related Phenomena

www.elsevier.nl/locate/elspec

# Probing transient molecular structures with time-resolved pump/probe XAFS using synchrotron X-ray sources

Lin X. Chen\*

*Chemistry Division, Argonne National Laboratory, 9700 South Cass Avenue, Argonne, IL 60439, USA*

## Abstract

Laser pulse pump, X-ray pulse probe X-ray absorption fine structure (pump-probe XAFS) experiments using synchrotron sources are described from technical considerations and from scientific significance. There are three technical challenges of such experiments: (1) laser photoexcitation, (2) synchronization of laser pulse and X-ray pulse, and (3) detection; each of which is investigated in detail. Based on the results from these investigations, the transient molecular structure of a reaction intermediate produced by photoexcitation of NiTPP-L<sub>2</sub> (NiTPP, nickeltetraphenylporphyrin; L, piperidine) in solution has been captured for the first time with the pump-probe XAFS on a 14-ns time scale obtained from the X-ray pulses from a third generation synchrotron source. The experimental results confirm that photoexcitation leads to the rapid removal of both axial ligands to produce a transient square-planar intermediate, NiTTP, with a lifetime of 28 ns. The transient structure of the photodissociated intermediate is nearly identical to that of the ground state NiTPP, suggesting that the intermediate adopts the same structure as the ground state in a non-coordinating solvent before it recombines with two ligands to form the more stable octahedrally coordinated NiTPP-L<sub>2</sub>. No detectable population of a penta-coordinated intermediate was present. This experiment demonstrates the feasibility of determining transient molecular structures in disordered media using the temporal resolution of a synchrotron X-ray source. © 2001 Elsevier Science B.V. All rights reserved.

*Keywords:* XAFS; Pump-probe; Time-resolved XAFS; NiTPP; Synchrotron; Structures of intermediates

## 1. Introduction

Molecular structures are the bases of understanding photochemical reaction mechanisms and molecular reactivity. Although many aspects of photochemistry can be well understood based on the ground state structures, our understanding of the processes often remains incomplete due to unknown structures of transient molecular species, such as the excited states. When a molecule is excited by light, its electron density distribution is changed. Accord-

ing to the Franck–Condon principle, the initial reaction coordinates in the excited states remain the same as those in the ground state despite changes in the electron density distribution due to photoexcitation [1]. The nuclear coordinates will respond to the electron density change through various rapid relaxation processes, resulting in equilibrated excited state reaction coordinates that differ from those of the ground state (Fig. 1). In solution, the time required for the initial excited state nuclear coordinates to relax to the equilibrated excited state coordinates could be as long as a few vibrational cycles, or on femto to pico second time scales [2]. These excited states can proceed to form other transient states and the product, or they can return to the ground state.

\*Tel.: +1-630-252-3533; fax: +1-630-252-9289.

E-mail address: lchen@anl.gov (L.X. Chen).

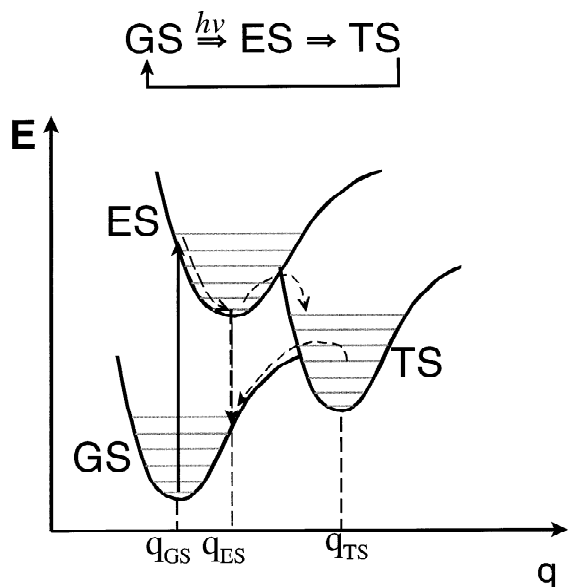


Fig. 1. Molecule interaction with light in a reversible reaction. The ground state (GS) molecules are excited to an excited state (ES) which undergoes fast relaxation to the equilibrated reaction coordinates  $q_{ES}$ , different from those of the GS,  $q_{GS}$ . The ES may proceed to other transient states (TS) or return to the GS directly. Very little information on  $q_{ES}$  and  $q_{TS}$  is known. The pump-probe XAFS aims to determine these structures during their short lifetimes.

The pump-probe experiment has been commonly used in laser spectroscopy [3–15], where a pump laser pulse triggers a reaction in the sample and a probe pulse monitors optical responses of the sample after the pump. Laser pump/probe spectroscopy reveals kinetics of the reactions as well as coherence between different states of the molecules involved in photochemical processes, but it cannot obtain structures of the molecules during the reactions. Consequently, the lack of knowledge in the transient structures of the molecules greatly hinders fundamental understanding of the origins of the functions. Therefore, developing parallel X-ray techniques to determine material structures during light-induced processes becomes necessary.

Significant progress has been made in recent years to generate ultrashort X-ray pulses [16–19] for following atomic movements from the initial Franck–Condon state to the equilibrated excited

state, as well as for capturing the molecular structures of other transient species. Some experiments have been carried out using bench-top laser plasma-based and synchrotron X-ray sources [20–22]. Because many photochemical reactions occur in disordered media, X-ray techniques that do not rely on the long-range order of the structure must be developed. Although the concept of laser pump/X-ray probe X-ray absorption fine structure (XAFS) using synchrotron radiation was proposed earlier [23–25], transient molecular structures generated in light-induced processes were mainly captured in the past without using the temporal resolution of the source [26–34].

We report here our effort in determining transient molecular structures during photochemical reactions by pump-probe XAFS using a third generation synchrotron X-ray source. Because the intrinsic time resolution of the pump-probe technique is determined by the pulse duration of the pump or the probe, whichever is longer, the synchrotron X-ray pulse will provide a time resolution of the order of 100 ps [35]. This time scale is apparently too long for monitoring the atomic movement from the initial Franck–Condon state to the equilibrated excited state, but it is suitable for capturing structures of the equilibrated excited states within their lifetimes ranging from 100 ps to longer. The structural information on these equilibrated excited states, as well as other transient species, is crucial to the fundamental understanding of the photochemistry.

The third generation synchrotron X-ray sources provide not only an X-ray brilliance several orders of magnitude higher than previous X-ray sources, but also novel timing structures of X-ray pulses [35]. The high X-ray brilliance and flux shorten the time required to collect structural data and the timing structures of the X-ray pulses allow extraction of the probe signals from a single X-ray pulse. Thus, the fs laser plasma-based and synchrotron-based X-ray sources are complementary in solving transient molecular structures on different time scales. In the following, we will discuss the challenges in the pump-probe XAFS using the synchrotron X-ray sources, and our recent work on the determination of a transient molecular structure during a photodissociation process.

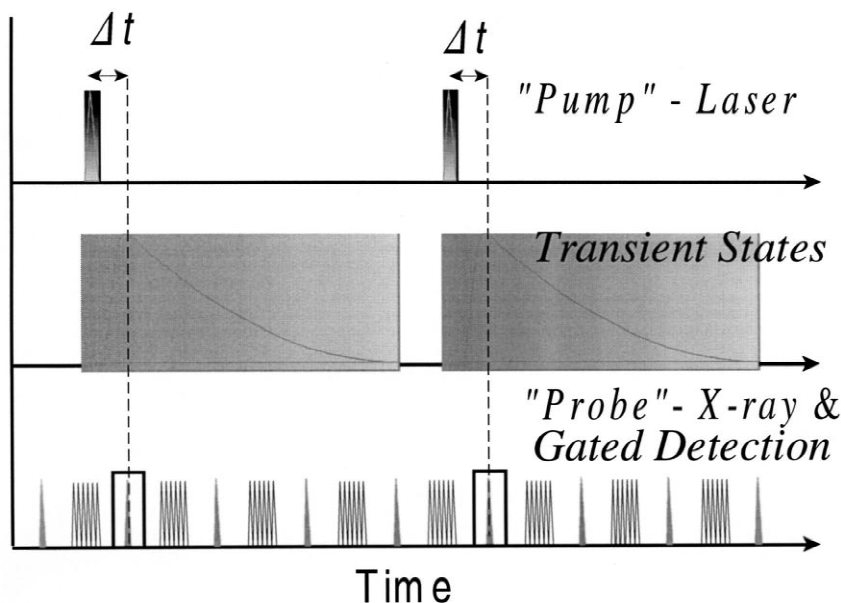


Fig. 2. Time sequence of the pump-probe XAFS.

## 2. Experimental methods

Fig. 2 demonstrates the timing sequence of the pump-probe XAFS, as well as key factors for the experiment. A laser pump pulse triggers a photochemical reaction. An X-ray pulse at a certain time delay from the trigger,  $t$ , is used to probe the structure of the molecules. In addition, an X-ray detector is synchronously gated with the probe X-ray pulse to selectively collect signals only at the instant when the concentration of the transient species of interest is at its maximum after each excitation pump pulse. The pump-probe cycle can be repeated until a sufficient signal/noise ratio of the spectrum is reached.

### 2.1. Photoexcitation requirements

One of the key requirements for the experiment is the number of photons from each laser pulse. Because it is rare to have 100% photoexcitation of the molecules, XAFS measures a mixture of the ground and the excited states. Therefore, the larger the

fraction of the excited state molecules, the more likely the transient structure can be determined. The fraction of the excited state molecules  $f_{\text{ex}}$  is a function of the laser pulse energy  $P$ , the extinction coefficient of the molecule at the wavelength of the laser light,  $\varepsilon$ , the quantum yield  $Q$ , as well as the sample geometry. Eq. (1) describes the relationship between  $f_{\text{ex}}$  and other experimental factors at a time  $t$  after the pump pulse:

$$f_{\text{ex}} = \frac{N_a \cdot e^{-kt} \cdot Q}{N} = \frac{P \cdot e^{-kt} \cdot Q}{N \cdot h\nu} \cdot [1 - 10^{-\varepsilon(\lambda)lC(1-f_{\text{ex}}Q \cdot e^{-kt})}] \quad (1)$$

where  $N$  and  $N_a$  are the total number of molecules, and the number of molecules that absorb the light, respectively;  $k$  is the excited state decay time constant, and  $t$  is the time after the pump.  $Q$  is the quantum yield of the excitation.  $P$  is the pulse energy of the laser,  $h$  is the Planck constant, and  $\nu$  is the frequency of the laser light.  $C$  and  $l$  are the concentration and the thickness of the sample. Eq. (1)

assumes that the excited state decay follows a single exponential function and  $l$  is small enough so that the absorption gradient through the pathway of the light can be neglected. Fig. 3 gives two examples of calculated  $N_a/N$  as a function of  $\varepsilon$  and  $C$  at  $t=0$ , and indicates that as  $\varepsilon$  gets smaller and  $C$  increases, it becomes more and more difficult to excite a significant fraction of the molecules. Using the results from these calculations, we can estimate  $f_{ex}$  at  $t=0$ . The experimental condition and geometry in the pump-

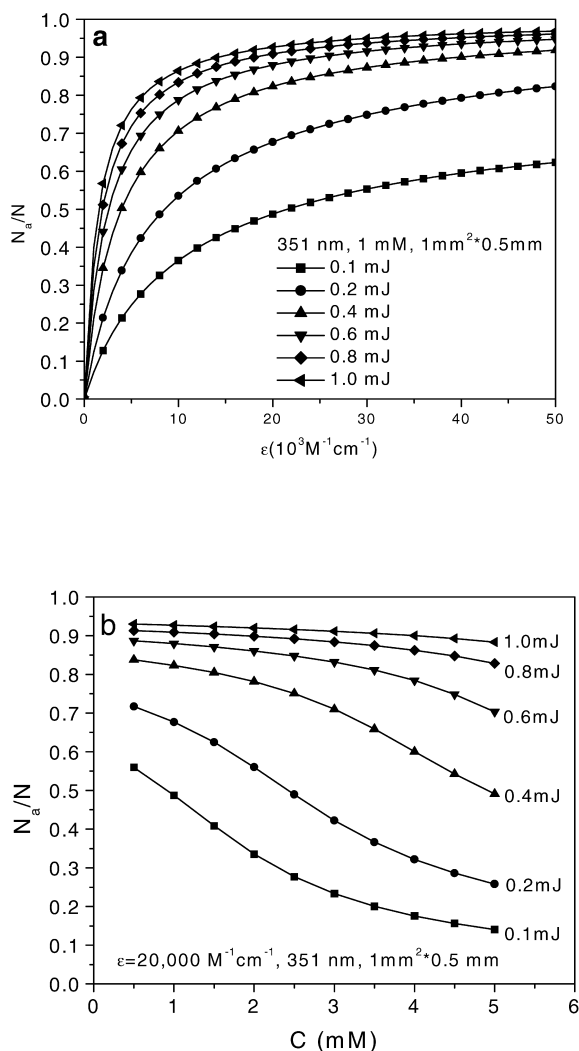


Fig. 3. The fraction of molecules that absorb light as functions of (a), (8) when  $C$  and  $\varepsilon$  are fixed and (b)  $C$  when, (8) and  $\varepsilon$  are fixed, at different laser pulse energies.

probe XAFS experiment can be chosen using Eq. (1) as a guide.

An ideal laser system to serve as the pump for photo-initiated processes should have a high repetition rate, a high pulse energy, short pulse width (FWHM), and a broad tunability in UV and visible regions. However, the high pulse energy from a laser inevitably limits the repetition rate of the laser. In our current experimental set-up, the laser repetition rate is 1–2 kHz whereas that of the X-ray pulse is of the order of a few MHz. Consequently, the usable X-ray flux for the pump-probe XAFS experiment is reduced by a factor of 1000–2000. This is one of the challenges that the synchrotron pump-probe XAFS is facing, which also warrants the need for the high X-ray flux from the third generation synchrotron sources.

## 2.2. Synchronization requirements

Another important factor of the pump-probe XAFS experiment is the timing structure of the X-ray pulses and the synchronization of the laser pump pulse with the X-ray probe pulse. The repetition rate of the pump-probe cycle is limited by the recovery time of the reaction and of the detector, as well as the repetition rate of the pump laser pulses. These limitations result in a much lower repetition rate for the pump-probe cycle than that of the X-ray pulses from a synchrotron source. Consequently, the signal from a single X-ray pulse that immediately follows the pump laser pulse must be extracted. Although a much larger circumference of the storage ring of the third generation source is potentially capable of providing a much larger time window for extracting the signals from a single X-ray pulse, it is not practical to have only one single electron bunch circulating in the storage ring. In practice, an asymmetric fill pattern of the electron bunches is implemented where the total number of electron bunches remains large, but one of the electron bunches is well separated in time from the others [36]. In order to extract a single X-ray pulse or a group of pulses, several X-ray shutters have been designed and constructed for time-resolved studies [36–38]. The slow speed shutters are made of fast rotating metal blades and can be used to extract a part of an X-ray pulse train with sub-millisecond

opening time. The intermediate speed shutter with a rotating polygon mirror is capable of extracting X-ray pulses with one microsecond opening and can be used to extract a single pulse during the asymmetric fill operation [38]. The fast speed shutter is a rotating Si single crystal cube with a pair of slits in the distance [37], extracting a single X-ray pulse with a sub- $\mu$ s opening. With all the designs available, extracting a single X-ray can be achieved at various synchrotron sources. Our current experiments, however, did not use any X-ray shutter. Alternatively, a gated detection scheme has been implemented and will be described below.

The synchronization of the laser pulse with the X-ray pulses from the synchrotron has been accomplished by three-stage delays in our experiments shown in Fig. 4. Under the asymmetric fill operation, an electron bunch, so-called ‘superbunch’, is in the middle of a 3.16  $\mu$ s time window at the Advanced Photon Source (APS) at Argonne National Labora-

tory. The laser system used in our experiments consists of a mode-locked, diode-pumped Nd-YLF laser (Lightwave, LW-131) driven by 1/4 of the frequency of the RF signal of the storage ring. The pulses from this seed laser at  $\sim 88$  MHz are thus intrinsically synchronized to the X-ray pulses. The seed laser pulses are injected and selectively amplified by a Nd-YLF regenerative amplifier laser (Quantronix). The Q-switch (Medoxx) of the laser is triggered at 1 kHz by a signal that is delayed and frequency-divided from the ring revolution signal  $P_0$  of 271 kHz. By changing the delay between the Q-switch of the laser relative to  $P_0$ , the first delay determines which superbunch is used to overlap with one of the laser pulses. Because the 1 kHz laser pulses are selected from the 88 MHz seed laser pulse train, the first delay adjustment has a precision limited to 11.35 ns that separates two adjacent seed laser pulses. The second delay adjusts the phase difference between the RF signal and the sinusoidal

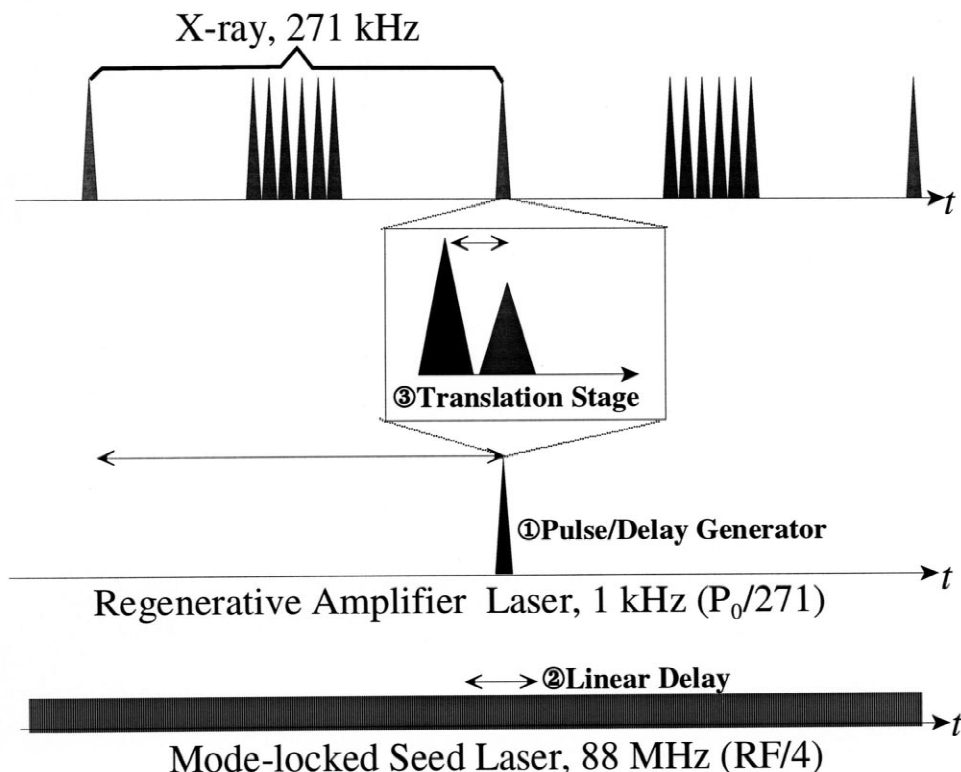


Fig. 4. Three-stage synchronization between the laser and the X-ray pulses.

signal driving the mode-locked laser to 1 ns precision by a linear delay generator. The third delay varies the optical path of the laser pulses through an optical delay line, which can reach a sub-picosecond precision. However, the time precision for the overlap in our present experimental set-up is limited by the response time of a photodiode detector monitoring the laser and the X-ray pulses and is less than 100 ps.

### 2.3. Detection requirements using a Ge detector array

In order to obtain an analyzable spectrum with the pump-probe XAFS, an efficient detector needs to be selected and the detection scheme needs to be modified from that of the steady-state XAFS measurements. Many photochemical processes occur in dilute solutions, so excited state quenching and exciton–exciton annihilation can be prevented. In addition, most metalloproteins with interesting photochemical properties have intrinsically dilute metal concentration. Thus, the X-ray fluorescence detection must be used for most of the pump-probe XAFS experiments. The basic requirements for the X-ray fluorescence detector for the experiments are (1) an energy resolution allowing separation of fluorescence signals of a specific element from those of elastic scatterings and fluorescence of other elements with similar atomic numbers, (2) a capability of synchronized detection with the X-ray probe pulses, (3) a large solid angle to effectively collect the signals from a dilute sample, and (4) a fast enough response time to eliminate interference of other X-ray pulses to the signals of the gated probe pulse. Although different X-ray fluorescence detectors are available for dilute samples [39–48], most of these detectors have not been used for the pump-probe XAFS. A multi-element Ge solid state detector (Canberra) [44], which is known to fulfil the first three requirements, was used in our experiment. However, the last requirement for the detector has not been investigated thoroughly because few precedent experiments have been carried out in such a manner. Issues in the detector application are addressed here: (1) effects of multi-photons from a single X-ray pulse, (2) the optimized number of

detected photons, (3) detector gating, and (4) timing requirement. The high photon flux within a single X-ray pulse from the third generation synchrotron enables us to conduct the pump-probe XAFS experiment, but some problems of detection also arise due to such a high flux. For example, the incident X-ray flux at 11ID-D wiggler beamline of the APS is about  $5.5 \times 10^{11}$  photons/s at 9 keV at the sample when the total storage ring current is 100 mA. During the asymmetric fill operation, the current in the superbunch is 15 mA. Therefore, the incidental photon flux from the superbunch is  $8.3 \times 10^{10}$  photons/s or  $3.0 \times 10^5$  photons/pulse at 9 keV. In contrast, a bending magnet beamline at a second generation synchrotron source provides  $10^9$  photons/s at the sample or about 23 photons/pulse at 8 keV, a factor of 13,000 smaller than the superbunch at the wiggler beamline at the APS. The superbunch under the current hybrid mode operation in the APS is a cluster of six single pulses with a 2.84-ns separation between adjacent pulses. If a single pulse within the six-pulse cluster in the superbunch is concerned, there is a factor of 2000 increase in the number of X-ray photons in a single pulse at a wiggler beamline at APS compared to that at a bending magnet beamline at a second generation source. An undulator beamline in the APS has a factor of 50–100 higher photon flux than the present state of the wiggler beamline at 11ID-D at the APS. Therefore, a pile-up problem for the detector could arise with such an increase in the photon flux. In order to assess the problem, an actual number of detected X-ray fluorescence photons from the sample needs to be calculated by the equation:

$$I_f = I_a \cdot \frac{\Omega}{4\pi} \cdot \eta \cdot \frac{\mu_k}{\mu_T} \cdot \eta_{\text{det}} \quad (2)$$

where  $I_f$  is the number of fluorescence photons,  $I_a$  is the number of photons absorbed by the sample,  $\Sigma$  is the solid angle covered by the detector,  $\eta$  is the quantum yield of the fluorescence,  $\mu_k$  and  $\mu_T$  are the absorption cross sections for the central absorbing element and for the entire sample, respectively.  $\eta_{\text{det}}$  is the detector efficiency defined as the fraction of the fluorescence photons in the total number of photons entering the detector. Because there are  $3 \times 10^5$  photons in one superbunch and the pump-

probe cycle is currently running at 1 kHz, the number of incident X-ray photons that will be used is  $3 \times 10^8$  photons/s. For a 1 mM Ni-containing sample with 1 mm<sup>2</sup> area and 0.5 mm thickness, about 15% photons will be absorbed, which gives  $I_a$   $4.5 \times 10^7$  photons/s. The solid angle  $\Omega/4\pi$  is 2.9% for a nine-element detector with a 9-cm<sup>2</sup> detection area situated 5 cm from the sample. The fluorescence quantum yield  $\eta$  for Ni is 70%, and the fraction of Ni absorption from the total absorption is 0.6%. With all the above factors considered, there would be 5500 X-ray fluorescence photons per second entering the detector, or 5.5 photons/superbunch.

The probability of  $k$  photon events for each of the  $m$  elements in the detector array is known to follow a Poisson distribution assuming that the total number of incidental photons is  $N$ ,

$$P(k, N, m) = \frac{(N/m)^k}{k!} \times e^{-N/m}. \quad (3)$$

The number of single photon events for the entire  $m$ -element array is then  $n_s(N, m) = mP(1, N, m)$ . Fig. 5 displays numbers of one-, two- and three-photon events as a function of  $N$  for a nine-element detector. When  $N=9$ , the single photon event detected is at the maximum of 3.7, while two-photon events are at

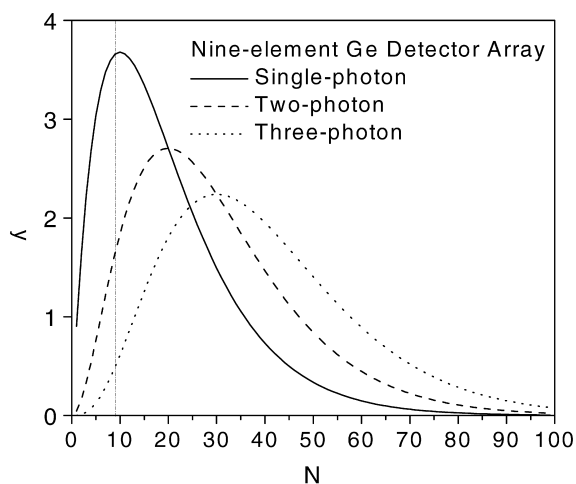


Fig. 5. The number of single-, two- and three-photon events vs. the number of incidental photons  $N$  for a nine-element solid state Ge detector array calculated by Eq. (3).

1.7 and three-photon events are at 0.6 by a nine-element detector. This implies that only 41% incidental photons can be collected as single photon events that will contribute to the useful signals for the XAFS spectrum. However, the detector is highly nonlinear at  $n_s=3.7$ , so the maximum allowed single photon event should be much lower. According to Fig. 5, the nonlinearity of the detector can be largely neglected when  $n_s < 3$ , corresponding to  $N < 5$ , giving a maximum of 33% of incidental photons to be collected as single photon events.

However, only part of the incidental photons contributes to the XAFS spectrum. A Ge solid state detector detects both elastic scattering and fluorescence photons. As a commonly encountered problem in collecting XAFS spectra of dilute samples, the elastic scattering photons often exceed the fluorescence photons by a factor of  $>100$ . This situation makes the solid state Ge detector impossible to use. The obstacle can be removed by using a combination of the Soller slits and a Z-1 filter from a Lytle Detector [49,50]. When a cobalt filter with six absorption lengths was used in our experiment at Ni K-edge with 1 mM NiTPP, the majority of the elastic scattering photons were blocked by this filter-slits combination, and the pile-up due to the elastic scattering photons was negligible. Although the cobalt fluorescence appeared as the result of this set-up, the fraction of Ni fluorescence photons was increased to 33% of the total photons entering the detector, whereas it was virtually invisible without the filter and the slits. In this case, the detector efficiency  $\eta_{\text{det}}$  is a product of the fraction maximum allowed single photon events and the fraction of the fluorescence photons, which gives 11% in our example. Therefore, a maximum number of effective fluorescence photons detected by a nine-element detector array is 400 photons/s at 1 kHz repetition rate. Consequently, the average integration time required to reach 100,000 counts/point is around 250 s. For an XAFS spectrum with 300 points, the total data acquisition time is 21 h. This result indicates the limitation of the multi-element solid state detector. The detector efficiency is severely reduced due to the elastic scattering from the sample. The detection in the pump-probe XAFS is detector-limited rather than photon flux-limited.

The gating of a Ge detector array can be accom-

plished by gating the amplifiers or the scaler. Based on our experimental results, a minimum of 1.2  $\mu\text{s}$  time separation is required to prevent interference between signals from adjacent X-ray pulses when the detector is operated with a 0.25  $\mu\text{s}$  shaping time. Such a time separation requirement could be reduced when a 0.125  $\mu\text{s}$  shaping time is used.

Recently, detectors for the dilute samples have been constructed with an angle-tuned multilayer coated Si crystal array [41] or with a bent Si single crystal [51]. These alternative detectors show a great potential in enhancing the detector efficiency by eliminating the elastic scattering photons. However, the applications of these detectors on the pump-probe XAFS remain to be further investigated.

### 3. A recent pump-probe XAFS study

Using the experimental set-up described above, we carried out a pump-probe XAFS experiment to capture the structure of a reaction intermediate with a 28-ns lifetime following the photodissociation of NiTPP- $L_2$  ( $L$ =piperidine) in solution (Fig. 6) at the 11ID-D wiggler beamline at APS. The photo-induced axial ligand dissociation/association processes of heme-like porphyrin derivatives are examples of how the coordination geometry of a metal ion can be altered by the electronic structure of its macrocycle ligands, and serves as a model for oxygen transportation, catalysis, and photoinduced redox reactions.

According to previous studies [52–54] (Fig. 6),

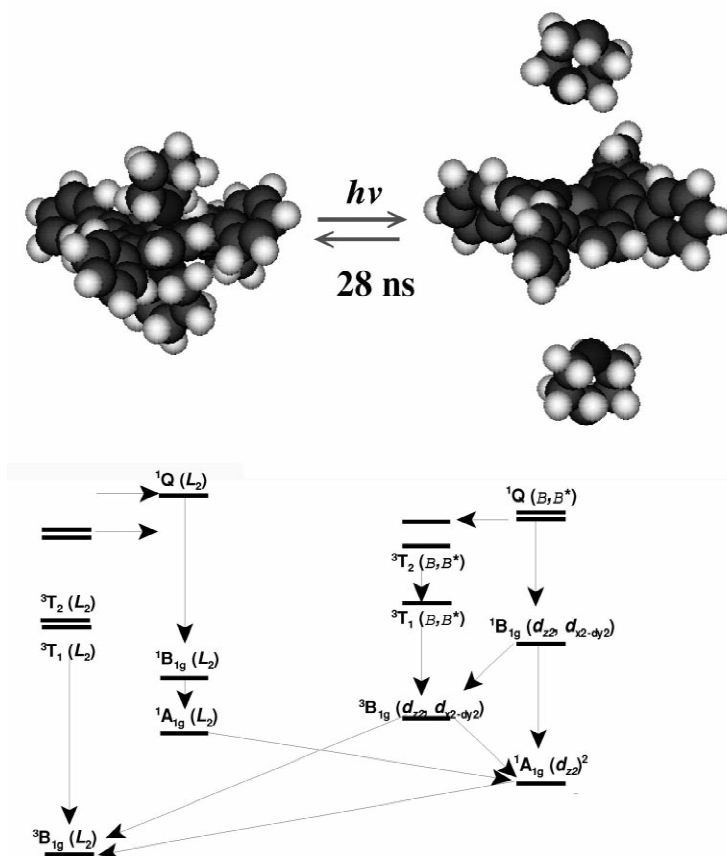


Fig. 6. Photodissociation/photoassociation reaction of NiTPP. The reaction is reversible and both photodissociation/association can be triggered by the laser excitation.

the  $3d^8$  electrons of Ni(II) in a distorted square-planar NiTPP molecule is mostly at a low spin  $(3d_{z^2})^2$  (the superscript indicates the electron occupancy of the molecular orbital) state in a weakly coordinating and non-coordinating solvent, but are in a high spin  $(3d_{x^2-y^2}, 3d_{z^2})$  state with an octahedral coordination geometry binding two axial ligands in strongly coordinating solvents, such as piperidine. Photoinduced electronic  $\pi-\pi^*$  transitions of the porphyrin macrocycle in NiTPP initiate an electronic configuration change from  $(3d_{z^2})^2$  to  $^1(3d_{x^2-y^2}, 3d_{z^2})$  (superscript on the left of parenthesis indicates the electron spin state), then an inter-system crossing from  $^1(3d_{x^2-y^2}, 3d_{z^2})$  to  $^3(3d_{x^2-y^2}, 3d_{z^2})$ , which favors octahedral coordination geometry, leading to the photoassociation of the two axial ligands in weakly coordinating solvents. Conversely, similar  $\pi-\pi^*$  excitation of NiTPP- $L_2$  ( $L$ =axial ligand) is followed by a cascade decay of upper excited states, leading to a transition from  $^3(3d_{x^2-y^2}, 3d_{z^2})$  to  $^3(3d_{z^2})^2$  and an inter-system crossing to a low spin singlet  $^1(3d_{z^2})^2$  state which is stabilized by a square planar coordination geometry, causing the dissociation of the two axial ligands.

The excited state dynamics for NiTPP have been studied extensively by ultrafast time-resolved optical transient absorption and Raman spectroscopies [52,55,56]. Although the processes of the excited state interconversion in NiTPP- $L_2$  are on time scales of femto- to picoseconds [52,55], the intermediate from the photodissociation has a lifetime of over 25 ns (Fig. 7) in a neat piperidine solution before it recombines with two piperidine ligands and returns to the  $^3(3d_{x^2-y^2}, 3d_{z^2})$  ground state. Fig. 8 shows possible pathways for the recovery of the photodissociated NiTPP back to the ground state NiTPP- $L_2$ . Starting with NiTPP- $L_2$ , a laser pump pulse induces an electronic transition from the triplet ground state,  $T_0$ , to a group of excited triplet states,  $T^*$ . These states decay and undergo inter-system crossing to an excited singlet state,  $S^*$ . This excited state subsequently reacts by ejecting two ligands to produce the square-planar geometry to  $S_0$  [52–54]. If the solvent were non-coordinating or weakly coordinating this reaction sequence would be completed. However, in a strongly coordinating solvent the singlet state is unstable and the system will return to

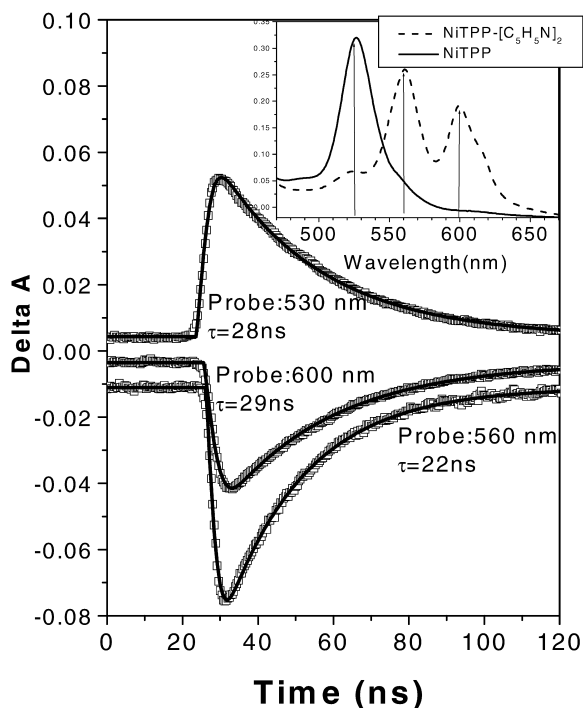


Fig. 7. The photodissociation kinetics measured by optical pump-probe transient absorption. The inset is a part of the optical absorption spectra of NiTPP and doubly ligated NiTPP- $L_2$  ( $L$ = piperidine,  $C_5H_5N$ ). The kinetics were monitored at the characteristic absorption peaks for the molecules. At 530 nm, the growth of photodissociated NiTPP is monitored, and at 560 and 600 nm, the depletion of NiTPP-(piperidine) $_2$  is monitored. The optical transient absorption result at 530 nm suggests that 28% NiTPP-(piperidine) $_2$  was photodissociated.

the ground triplet state,  $T_0$ , by recombining with two piperidine ligands to form an octahedrally coordinated NiTPP- $L_2$ . The transient structures involved in this recombination are not known. A penta-coordinated NiTPP- $L$  molecule could be involved in the recombination, the square-planar NiTPP could return to  $T_0$  via a concerted axial chelation with two piperidine molecules, or an intermediate square pyramid NiTPP- $L$  structure could be important. Because it is difficult to identify uniquely the optical absorption spectrum for each possible intermediate involved in photodissociation, transient optical absorption spectra of NiTPP in coordinating solvent alone are not sufficient to identify the intermediates,

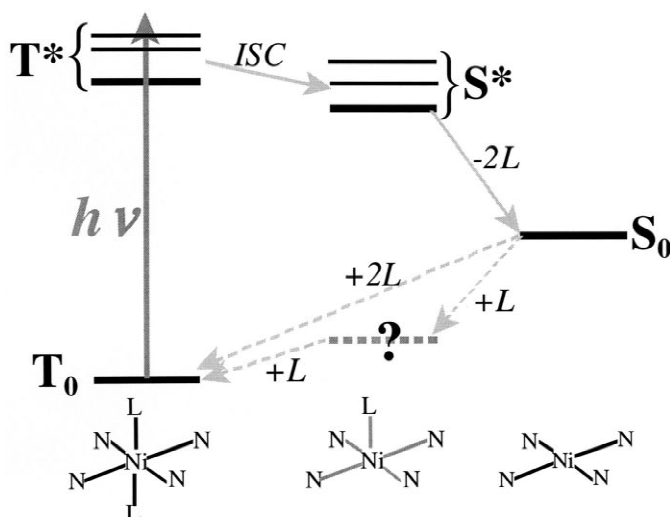


Fig. 8. Reaction path of photodissociation of NiTPP- $L_2$ , (only the nearest neighboring atoms that are chelated with Ni are shown) where the ground triplet state  $T_0$  is photoexcited to upper triplet states  $T^*$  (representing a group of possible triplet states).  $T^*$  then undergo intersystem crossing to  $S^*$ , which could occur very quickly, and, finally, ejection of two ligands to form  $S_0$ . This transient species was captured by the laser pump/X-ray probe XAFS experiment before it returned to the more stable  $T_0$  state of NiTPP- $L_2$ .

whereas transient XAFS may be used to directly obtain the coordination geometry of the Ni atoms and, therefore, identify the intermediates.

### 3.1. Specific experimental conditions

The pump-probe XAFS experiment presented in the following section was conducted at the Ni K-edge (8.333 keV). The energy of the X-rays was selected by a cryogenically cooled fixed offset double crystal Si(220) monochromator on the wiggler beamline 11ID-D, BESSRC-CAT at APS. To achieve complete coverage by the pump laser of the sample probed by the X-rays, the X-rays were focused by a Pd toroidal mirror to a beam size of  $0.5 \times 1 \text{ mm}^2$  at the sample, which is less than the laser beam diameter of 2 mm. The experiment was carried out during the special operating mode when the asymmetric fill pattern of the storage ring was implemented. The electron superbunch generates six X-ray pulses within 14.2 ns (2.84 ns between pulses), and this six-pulse cluster is separated by 1580 ns on each side from other pulses. The laser pump pulses are at 351 nm, with an average pulse energy of 0.8 mJ. The kinetics of the reaction is measured by a transient optical absorption set-up,

using the same laser as the pump and a xenon flash lamp as the probe. The decay profile may be fit with a single exponential function  $A \exp(-t/\tau)$ , where  $\tau = 28 \text{ ns}$ . NiTPP (Aldrich) was dissolved in piperidine (Aldrich) to make a 1 mM solution. A multi-element solid state Ge detector (Canberra) with a  $0.25\text{-}\mu\text{s}$  shaping time was used to collect the Ni  $K_{\alpha}$  fluorescence. The outputs from the detector amplifiers were fed to single channel analyzers (SCAs), which were coupled to two scaler arrays interfaced with a computer. One of these arrays was gated with the laser pulses and the other was not gated or was gated  $14.73 \mu\text{s}$  later (four periods of the storage ring).

### 3.2. Results and discussion

The XAFS spectra are displayed in Figs. 9–12 for the laser pumped NiTPP- $L_2$  along with those of the ground state NiTPP- $L_2$  and NiTPP. A distinct shoulder at 8.340 keV appears in the X-ray absorption near edge structure (XANES) of the laser pumped sample (Fig. 9), which resembles a similar feature in the ground state NiTPP, and is attributed to the  $1s \rightarrow 4p_z$  transition in a square-planar complex [57]. This feature was not observed when the laser beam was

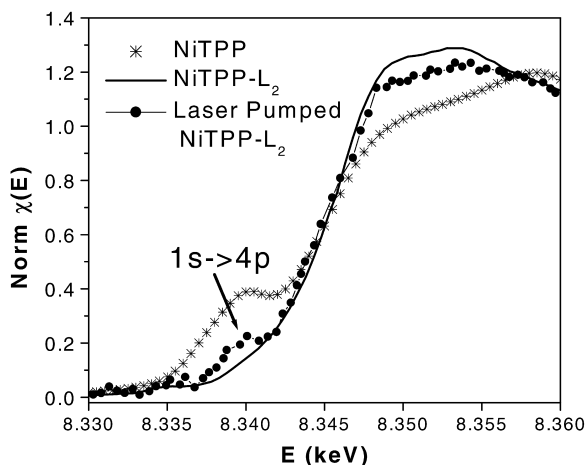


Fig. 9. Normalized X-ray absorption  $\mu(E)$  at the near edge as a function of X-ray energy,  $E$ . The shoulder at 8.340 keV for the laser-pumped sample is indicated by the arrow. The spectrum for the laser-pumped sample can be approximated by mixing the ground state spectra of NiTPP- $L_2$  and NiTPP in a ratio of 7:3.

blocked nor when the detector was gated at a time long after the ground state recovery. Therefore, the appearance of this feature indicates that both axial ligands are removed immediately after photoexcitation, forming a transient square planar NiTPP. The rest of the spectrum also exhibits differences from

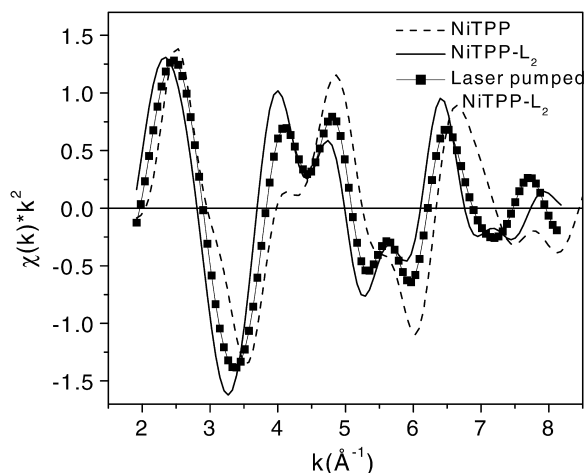


Fig. 10. Background-removed, Fourier transform-filtered XAFS spectra  $c(k)$  as a function of the wave vector  $k$  weighted by  $k^2$ , where  $\Pi(k) \propto 3N_j / (kR_j^2) \exp(-2\Phi_j^2 k^2) \sin[2kR_j + \phi_j(k)]$  ( $N_j$  is the coordination number,  $R_j$  is the average distance,  $\Phi_j$  is the Debye-Waller factor, and  $\phi_j$  is the phase shift).

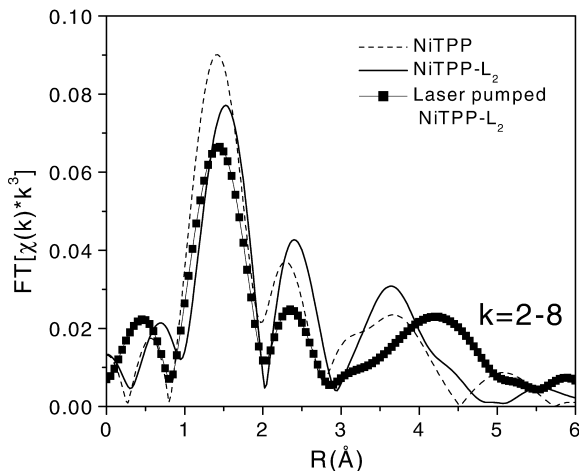


Fig. 11. Fourier transformed XAFS spectra weighted by  $k^3$ .

the spectrum of the starting octahedral NiTPP- $L_2$  (Fig. 10). Analysis of both the XANES and XAFS spectra suggests that the laser-pumped spectrum can be best described as a linear combination of  $70 \pm 5\%$  NiTPP- $L_2$  ground state and  $30 \pm 5\%$  NiTPP-like intermediate, which is in agreement with our calculation for the excitation yield of 30% under our experimental conditions, as well as with the transient optical absorption measurement where the pump pulse with the same pulse energy depleted 28% of the peak absorption by the ground state NiTPP- $L_2$ .

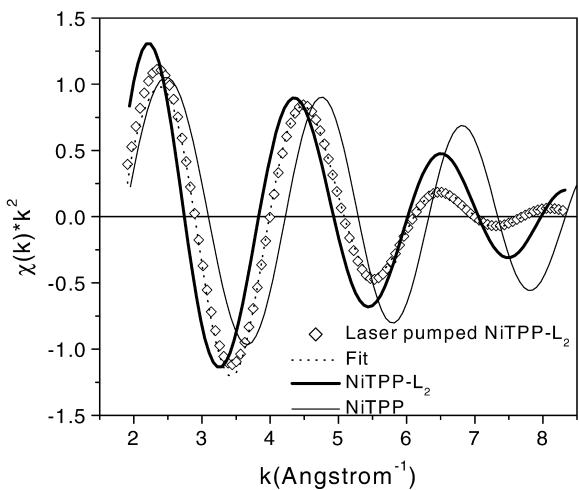


Fig. 12. The back Fourier transformed spectra for the nearest neighbors. The squares are the fits with the results shown in Table 1.

Fig. 11 shows the Fourier-transformed XAFS spectra, which indicate that the distances from the Ni ion to the nearest neighbor N atoms for the transient species are between those of NiTPP and NiTPP-L<sub>2</sub> at their respective ground states. Table 1 displays the nearest Ni–N distances obtained from a numerical analysis of these spectra. Each spectrum can be fit with a single Ni–N distance. The XAFS spectra for the nearest neighbors are shown in Fig. 12, along with the fit for the spectrum for the laser pumped sample. Table 1 lists the fitting results from the data analysis, and gives an average Ni–N distance of 1.91 Å for NiTPP, and 2.09 Å for NiTPP-L<sub>2</sub>, slightly deviated from the crystal structures, respectively [58]. The discrepancy between the solution and the crystal structures may arise from the dynamic nature of the ligation at room temperature in solution [58]. The nearest neighbors for the laser-pumped sample could be best described by two distances of 2.10±0.02 Å and 1.92±0.02 Å with a relative ratio of 3.2:1. This ratio is only slightly less than an expected value of 3.5:1 and within the experimental errors for a 30% yield of the square-planar intermediate. Based on structures of a previously studied penta-coordinated Ni bacterial chlorophyll that has a similar coordination environment as porphyrin, the Ni–N bond length increases from 1.95 to 2.04 Å when the coordination of Ni changes from a square-planar to a square-pyramid geometry [59]. Thus, if there were a substantial amount of NiTPP-L present, the nearest neighbor distances would not resemble as closely those for NiTPP and NiTPP-L<sub>2</sub>. Moreover, the fraction of the NiTPP intermediate obtained from fitting the XANES would not agree so well with the

two-distance fitting of the nearest neighbors from the XAFS spectra. In addition, the pre-edge peak of 1s-to-3d transition is not enhanced, as it would be in the non-central symmetric geometry of a square-pyramid NiTPP-L. Therefore, the photoinduced intermediate formed during the first 14 ns after the laser pulse is primarily the square-planar NiTPP with an average nearest neighbor distance that is almost identical to the ground state NiTPP. This result rules out the presence of a substantial amount of transient NiTPP-L. However, if the yield of NiTPP-L were less than 10% [54], only 3% of the total number of molecules, it would not have been properly detected. Moreover, if the lifetime of NiTPP-L were much shorter than the 14-ns duration of the superbunch, it would not have been observed.

These results agree with the previously proposed reaction path for the photodissociation of NiTPP-L<sub>2</sub> with a triplet ground state [54]. Upon excitation to an excited triplet state the system crosses to a singlet manifold, ejects two axial ligands, and relaxes to the singlet state S<sub>0</sub> within a few hundred picoseconds. Eventually it returns to the stable T<sub>0</sub> ground state via a thermally activated, diffusion-controlled process. There is no indication that the association of the axial ligands occurs in a step-wise process where NiTPP-L would be seen as an intermediate.

#### 4. Conclusion

Our results demonstrate that laser pump/X-ray probe XAFS using X-rays from a third generation synchrotron source provides a new and powerful

Table 1  
The nearest neighbor distances in NiTPP<sup>a</sup>

Compound	Coordination number	Bond length (Å)	Debye–Waller <sup>b</sup> factor (Å <sup>2</sup> )
NiTPP	4.0±0.5	1.91±0.02	0.003
NiTPP-(piperidine) <sub>2</sub>	6.0±0.5	2.09±0.02	–0.003
Laser pumped NiTPP-(piperidine) <sub>2</sub>	5.7±0.5	2.10±0.02	0.004
	1.8±0.5	1.92±0.02	0.005

<sup>a</sup> Feff7.0 from University of Washington [60] was used to calculate the reference spectra for NiTPP and NiTPP-(piperidine)<sub>2</sub> based on their crystal structures respectively [61,62]. WinXAS 97 [63] was used for data analysis.

<sup>b</sup> Relative to the crystal structures.

approach to monitor transient molecular structures in disordered media. For many metal-containing photoactive molecules, one of the most important electronic transitions that govern reactivity is the metal-to-ligand-charge-transfer (MLCT) transition, which involves moving electrons from the metal ion to ligands, producing a transient change in the oxidation state of the metal ion. This change could be detected by XAFS spectroscopy if the laser pump/X-ray probe technique can be applied. Inevitably, such transient oxidation changes could cause atomic displacements as well, which could also be detected by XAFS. Although the superbunch used in this experiment had six consecutive pulses within a 14-ns time span that limited the time resolution of this experiment, a single pulse superbunch is scheduled for future operation at the Advanced Photon Source and will allow us to capture intermediate structures on even shorter time scales.

### Acknowledgements

The work is supported by the Division of Chemical Sciences, Office of Basic Energy Sciences, US Department of Energy under contract W-31-109-Eng-38. The author would like to thank all the collaborators over the past 10 years on the time-resolved pump-probe XAFS and related projects. They are Drs. James R. Norris, Farrel W. Lytle, Marion Thurnauer, Pedro Montano, Michael K. Bowman, Michael R. Wasielewski, Zhiyu Wang, Peter L. Lee, Wighard J.H. Jäger, David J. Gosztola, Guy Jennings, Anneli Munkholm, and Jan Hessler. This work would not be possible without their support and participation. I would also like to express my sincere appreciation to all the staff members at BESSRC-CAT, Advanced Photon Source for their technical assistance.

### References

- [1] P.W. Atkins, in: *Quanta*, Oxford University Press, Oxford, 1991, p. 133.
- [2] A.H. Zewail, *J. Phys. Chem. A* 104 (2000) 5660.
- [3] P. Kambhampati, D.H. Son, T.W. Kee, P.F. Barbara, *J. Phys. Chem. A* 104 (2000) 10637.
- [4] U. Neukirch, S.R. Bolton, L.J. Sham, D.S. Chemla, *Phys. Rev. B: Condens. Matter Mater. Phys.* 61 (2000) R7835.
- [5] M. Dahlbom, T. Minami, V. Chernyak, T. Pullerits, V. Sundstroem, S. Mukamel, *J. Phys. Chem. B* 104 (2000) 3976.
- [6] J.Y. Bigot, V. Halte, J.C. Merle, A. Daunois, *Chem. Phys.* 251 (2000) 181.
- [7] P. Hamm, M. Lim, W.F. DeGrado, R.M. Hochstrasser, *J. Chem. Phys.* 112 (2000) 1907.
- [8] S. Link, C. Burda, B. Nikoobakht, M.A. El-Sayed, *Chem. Phys. Lett.* 315 (1999) 12.
- [9] A. Kummrow, M.F. Emde, A. Baltuska, M.S. Pshenichnikov, D.A. Wiersma, *Z. Phys. Chem. (Muenchen)* 212 (1999) 153.
- [10] S. Savikhin, D.R. Buck, W.S. Struve, R.E. Blankenship, A.S. Taisova, V.I. Novoderezhkin, Z.G. Fetisova, *FEBS Lett.* 430 (1998) 323.
- [11] R. Monshouwer, A. Baltuska, F. van Mourik, R. van Grondelle, *J. Phys. Chem. A* 102 (1998) 4360.
- [12] T. Kobayashi, M. Kim, M. Taiji, T. Iwasa, M. Nakagawa, M. Tsuda, *J. Phys. Chem. B* 102 (1998) 272.
- [13] D.M. Jonas, G.R. Fleming, *Ultrafast Processes Chem. Photobiol.* (1995) 225.
- [14] S. Lin, H. Van Amerongen, W.S. Struve, *Biochim. Biophys. Acta* 1140 (1992) 6.
- [15] W.T. Pollard, S.Y. Lee, R.A. Mathies, *J. Chem. Phys.* 92 (1990) 4012.
- [16] R.W. Schoenlein, S. Chattopadhyay, H.H.W. Chong, T.E. Glover, P.A. Heimann, C.V. Shank, A.A. Zholents, M.S. Zolotorev, *Science (Washington, DC)* 287 (2000) 2237.
- [17] I.V. Tomov, D.A. Oulianov, P. Chen, P.M. Rentzepis, *J. Phys. Chem. B* 103 (1999) 7081.
- [18] C. Rose-Petruck, R. Jimenez, T. Guo, A. Cavalleri, C.W. Siders, F. Raksi, J.A. Squier, B.C. Walker, K.R. Wilson, C.P.J. Barty, *Nature (Lond.)* 398 (1999) 310.
- [19] C. Rischel, A. Rousse, I. Uschmann, P.-A. Albouy, J.-P. Geindre, P. Audebert, J.-C. Gauthier, E. Forster, J.-L. Martin, A. Antonetti, *Nature (Lond.)* 390 (1997) 490.
- [20] B. Perman, V. Srajer, Z. Ren, T.-Y. Teng, C. Pradervand, M. Wulff, R. Kort, K. Hellingwerf, K. Moffat, *Science (Washington, DC)* 279 (1998) 1946.
- [21] B. Winter, J. Gatzke, T. Quast, I. Will, M.T. Wick, A. Liero, D. Pop, I.V. Hertel, *Proc. SPIE-Int. Soc. Opt. Eng.* 3451 (1998) 62.
- [22] H. Oyanagi, A. Kolobov, K. Tanaka, *J. Synchrotron Radiat.* 5 (1998) 1001.
- [23] D.M. Mills, *Phys. Today* 37 (1984) 22.
- [24] C. Bressler, M. Chergui, P. Pattison, M. Wulff, A. Filipponi, R. Abela, *Proc. SPIE-Int. Soc. Opt. Eng.* 3451 (1998) 108.
- [25] B.C. Larson, J.Z. Tischler, *Oxford Ser. Synchrotron Radiat.* 2 (1997) 137.
- [26] D.J. Thiel, P. Livins, E.A. Stern, A. Lewis, *Nature (Lond.)* 362 (1993) 40.
- [27] D.M. Mills, A. Lewis, A. Harootunian, J. Huang, B. Smith, *Science (Washington, DC)* 223 (1984) 811.
- [28] L. Powers, J.L. Sessler, G.L. Woolery, B. Chance, *Biochemistry* 23 (1984) 5519.
- [29] B. Chance, R. Fischetti, L. Powers, *Biochemistry* 22 (1983) 3820.

- [30] L.X. Chen, Z. Wang, J.K. Burdett, P.A. Montano, J.R. Norris, *J. Phys. Chem.* 99 (1995) 7958.
- [31] L.X. Chen, M.K. Bowman, Z. Wang, P.A. Montano, J.R. Norris, *J. Phys. Chem.* 98 (1994) 9457.
- [32] L.X. Chen, P.L. Lee, D. Gosztola, W.A. Svec, P.A. Montano, M.R. Wasielewski, *J. Phys. Chem. B* 103 (1999) 3270.
- [33] H. Wang, G. Peng, L.M. Miller, E.M. Scheuring, S.J. George, M.R. Chance, S.P. Cramer, *J. Am. Chem. Soc.* 119 (1997) 4921.
- [34] E.M. Scheuring, W. Clavin, M.D. Wirt, L.M. Miller, R.F. Fischetti, Y. Lu, N. Mahoney, A. Xie, J.-j. Wu, M.R. Chance, *J. Phys. Chem.* 100 (1996) 3344.
- [35] G.K. Shenoy, P.J. Viccaro, D.M. Mills, Argonne National Laboratory Report, ANL-88-9, 1988.
- [36] D.M. Mills, *Rev. Sci. Instrum.* 60 (1989) 2338.
- [37] A. McPherson, W.-K. Lee, D.M. Mills, *Proc. SPIE-Int. Soc. Opt. Eng.* 3451 (1998) 139.
- [38] A. McPherson, J. Wang, P.L. Lee, D.M. Mills, *J. Synchrotron Radiat.* 7 (2000) 1.
- [39] C. Karanfil, Z. Zhong, L.D. Chapman, R. Fischetti, G.B. Bunker, C.U. Segre, B.A. Bunker, *AIP Conf. Proc.* 521 (2000) 178.
- [40] Z. Zhong, D. Chapman, B. Bunker, G. Bunker, R. Fischetti, C. Segre, *J. Synchrotron Radiat.* 6 (1999) 212.
- [41] K. Zhang, G. Rosenbaum, G. Bunker, *J. Synchrotron Radiat.* 5 (1998) 1227.
- [42] C. Gauthier, J. Goulon, E. Moguiline, A. Rogalev, P. Lechner, L. Strueder, C. Fiorini, A. Longoni, M. Sampietro et al., *Nucl. Instrum. Methods Phys. Res. Sect. A* 382 (1996) 524.
- [43] L.R. Furenlid, H.W. Kraner, L.C. Rogers, S.P. Cramer, D. Stephani, R.H. Beuttenmuller, J. Beren, *Nucl. Instrum. Methods Phys. Res. Sect. A* A319 (1992) 408.
- [44] S.P. Cramer, O. Tench, M. Yocum, G.N. George, *Nucl. Instrum. Methods Phys. Res. Sect. A* A266 (1988) 586.
- [45] S.S. Hasnain, P.D. Quinn, G.P. Diakun, E.M. Wardell, C.D. Garner, *J. Phys. E* 17 (1984) 40.
- [46] M. Marcus, L.S. Powers, A.R. Storm, B.M. Kincaid, B. Chance, *Rev. Sci. Instrum.* 51 (1980) 1023.
- [47] E.A. Stern, S.M. Heald, *Nucl. Instrum. Methods* 172 (1980) 397.
- [48] E.A. Stern, S.M. Heald, *Rev. Sci. Instrum.* 50 (1979) 1579.
- [49] F.W. Lytle, R.B. Gregor, G.H. Via, J.M. Brown, G. Meitzner, *J. Phys. Colloq. C8* (1986) 149.
- [50] F.W. Lytle, R.B. Gregor, D.R. Sandstrom, E.C. Marques, J. Wong, C.L. Spiro, G.P. Huffman, F.E. Huggins, *Nucl. Instrum. Methods Phys. Res. Sect. A* 226 (1984) 542.
- [51] G.S. Knapp, M.A. Beno, K.J. Gofron, *Proc. SPIE-Int. Soc. Opt. Eng.* 3151 (1997) 300.
- [52] D. Kim, C. Kirmaier, D. Holten, *Chem. Phys.* 75 (1983) 305.
- [53] D. Kim, D. Holten, *Chem. Phys. Lett.* 98 (1983) 584.
- [54] J. Rodriguez, D. Holten, *J. Chem. Phys.* 92 (1990) 5944.
- [55] H.S. Eom, S.C. Jeoung, D. Kim, J.-H. Ha, Y.-R. Kim, *J. Phys. Chem. A* 101 (1997) 3661.
- [56] D. Kim, T. Sprio, *J. Am. Chem. Soc.* 108 (1986) 2099.
- [57] T.A. Smith, J.E. Penner-Hahn, M.A. Berding, S. Doniach, K.O. Hodgson, *J. Am. Chem. Soc.* 107 (1985) 5945.
- [58] S.L. Jia, J. Zhang, J.G. Ma, J.A. Shelnut, N.Y. Nelson, C.J. Medforth, K.M. Smith, in: *Book of Abstracts, 217th ACS National Meeting, Anaheim, CA, March 21–25, INOR, 1999.*
- [59] L.X. Chen, Z. Wang, G. Hartwich, I. Katheder, H. Scheer, A. Scherz, P.A. Montano, J.R. Norris, *Chem. Phys. Lett.* 234 (1995) 437.
- [60] J.J. Rehr, J. Mustre de Leon, S.I. Zabinsky, R.C. Alberts, *J. Am. Chem. Soc.* 113 (1991) 5135.
- [61] S.-L. Jia, W. Jentzen, M. Shang, X.-Z. Song, J.-G. Ma, W.R. Scheidt, J.A. Shelnut, *Inorg. Chem.* 37 (1998) 4402.
- [62] A.L. McLean, G.J. Foran, B.J. Kennedy, P. Turner, T.W. Hambley, *Aust. J. Chem.* 49 (1996) 1273.
- [63] T. Ressler, *J. Synchrotron Radiat.* 5 (1998) 118.